PERGAMON

International Journal of Heat and Mass Transfer 44 (2001) 3941–3952

International Journal of HEAT and MASS TRANSFER

www.elsevier.com/locate/ijhmt

The extended Graetz problem with piecewise constant wall heat flux for pipe and channel flows

B. Weigand [a,*], M. Kanzamar [b], H. Beer [c]

[a] *Institut für Thermodynamik der Luft- und Raumfahrt, Universität Stuttgart, Pfaffenwaldring 31, 70569 Stuttgart, Germany*
[b] *Fachgebiet Thermische Verfahrenstechnik, TU Darmstadt, Petersenstrasse 30, 64287 Darmstadt, Germany*
[c] *Fachgebiet Thermodynamik, TU Darmstadt, Petersenstrasse 30, 64287 Darmstadt, Germany*

Received 13 July 2000; received in revised form 11 December 2000

Abstract

Heat transfer in the thermal entrance region of a pipe or a parallel plate channel has been analysed for laminar and turbulent internal flow taking into account axial heat conduction effects in the fluid. The present paper shows an analytical solution for the problem of a piecewise uniform wall heat flux. The obtained exact analytical solutions for the extended Graetz problem are as simple and efficient to compute as the related solutions of the parabolic problem. The obtained results show the effect of axial heat conduction in the fluid for a semi-infinite as well as for a finite length of the heated sections.

1. Introduction

The analysis of heat transfer in the thermal entrance region in ducts has been widely considered. For laminar internal flows an extensive literature review is given by Shah and London [1]. Also for turbulent internal flows many theoretical and experimental studies are available in literature [2]. In many cases of technical interest the magnitude of the Peclet number in the flow is sufficiently large that axial heat conduction effects in the flow can be ignored. This simplifies drastically the complexity in solving the energy equation. On the other hand, axial heat conduction effects in the flow play an important role if the Peclet number is smaller. This is the case, for example, in compact heat exchangers, where liquid metals are used as working fluids.

Many investigations have been carried out which deal with the solution of the so-called "extended Graetz problem", which takes into account the axial heat conduction in the fluid. [1] contains a literature review of this subject. Hennecke [3] solved numerically the energy equation for a hydrodynamically fully developed laminar flow in a circular pipe. He showed the importance of axial heat conduction in the fluid for the cases of uniform wall temperature and uniform wall heat flux. He also considered one finitely heated zone. For an analytical solution of the extended Graetz problem, even in laminar flow, the problem arises that the associated eigenvalue problem for the energy equation is non-selfadjoint. This means that the resulting eigenvalues could at least in principle be complex and the eigenvectors could be incomplete. In order to overcome these problems, Hsu [4], who solved the energy equation for laminar pipe and channel flow with constant heat flux at the wall, constructed the solution of the problem from two independent series solutions for $x < 0$ and $x > 0$. Both the temperature distribution and the gradients were then matched at $x = 0$ by constructing a pair of orthogonal functions from the non-orthogononal eigenfunctions by using the Gram–Schmidt orthonormalisation procedure. Hence this method is complicated by expansions in term of eigenfunctions belonging to a non-selfadjoint operator.

Papoutsakis et al. [5] showed that it is possible to produce an entirely analytical solution to the extended Graetz problem for heat flux boundary conditions by decomposing the energy equation into a pair of first-order partial differential equations. This method has been used also by Papoutsakis et al. [6] for the case of

* Corresponding author. Tel.: +49-711-685-3590; fax: +49-711-685-2317.
E-mail address: bw@itlr.uni-stuttgart.de (B. Weigand).

0017-9310/01/$ - see front matter
PII: S0017-9310(01)00014-X

Nomenclature

a	thermal diffusivity, (m^2 s^{-1})
a_1, a_2	functions defined by Eq. (6)
A_j	constants
c_p	specific heat at constant pressure, (J kg^{-1} K^{-1})
D	hydraulic diameter, $4h$ (planar channel), $2R$ (circular pipe), (m)
ΔF	relative error, $(Nu_{\text{elliptic}} - Nu_{\text{parabolic}})/Nu_{\text{elliptic}}$
h	distance between the centreline and the wall (planar duct), (m)
k	flow index, 0 for a planar channel, 1 for a circular pipe
k	thermal conductivity, (W m^{-1} K^{-1})
l	mixing length, (m)
L	characteristic length, $L = h$ (planar duct), $L = R$ (circular pipe), (m)
L	matrix operator, Eq. (9)
$\tilde{n}$	coordinate, (m)
Nu_D	Nusselt number based on the hydraulic diameter, Eq. (37)
Nu_∞	Nusselt number for fully developed flow
p	pressure, (N m^{-2})
Pr	Prandtl number
Pe_D	Peclet number based on the hydraulic diameter
Pr_t	turbulent Prandtl number
$\dot{q}_w$	wall heat flux, (W m^{-2})
r	radial coordinate, (m)
R	pipe radius, (m)
Re_D	Reynolds number based on the hydraulic diameter
T	temperature, (K)
T_0	uniform temperature for $x \to -\infty$, (K)
T_b	bulk temperature, Eq. (36), (K)
u	axial velocity, (m s^{-1})
$\bar{u}_0$	axial mean velocity, (m s^{-1})
x	axial coordinate, (m)
x_1	end of the heated section, (m)
$\tilde{x}$	dimensionless coordinate, Eq. (3)

Greek symbols

ε_{hx}	eddy diffusivity in axial direction, (m^2 s^{-1})
ε_{hn}	eddy diffusivity in normal direction, (m^2 s^{-1})
ε_m	eddy kinematic viscosity, (m^2 s^{-1})
r	density, (kg m^{-3})
λ_j	eigenvalue
θ	dimensionless temperature
θ_b	dimensionless bulk temperature
θ_∞	fully developed temperature profile
v	kinematic viscosity, (m^2 s^{-1})
Σ	axial energy flow, Eq. (7)
$\vec{\Phi}_j$	eigenfunction

constant wall temperature in laminar pipe flow. Unfortunately only some temperature profiles have been shown in [5], but no plots of the Nusselt number are given. Nguyen [7] and Bilir [8] investigated numerically the heat transfer for thermally developing flows in a circular pipe and between parallel plates. Nguyen [7] derived from his computational results accurate engineering correlations for the Peclet number effect on the local Nusselt number and the thermal entrance length.

Although axial heat conduction can be ignored for turbulent convection in ordinary fluids and gases, that is often not the case when using liquid metal as the working fluid. This is because of the very low Prandtl number for this type of fluid ($0.001 < Pr < 0.06$). Thus, the Peclet number can be smaller than five in turbulent duct flows where liquid metals are used. A literature review concerning heat transfer in liquid metals can be found in [9]. Lee [10] studied the extended Graetz problem in turbulent pipe flow for constant wall heat flux for a semi-infinite heated section ($x > 0$). He used the turbulent Prandtl number model of Azer and Chao [11] for his study. Lee used the method of Hsu [4] to obtain a series solution for the problem. Therefore, the resulting solution is plagued by the same uncertainties as the one in [4]. Weigand [12] investigated analytically the extended turbulent Graetz problem with Dirichlet wall boundary conditions for a circular pipe and a parallel plate channel. He used the method developed by Papoutsakis et al. [6] for laminar pipe flow and extended the method to turbulent flow by using a newly defined vector norm. This method is not plagued by any uncertainties arising from expansions in terms of eigenfunctions belonging to a non-selfadjoint operator. In the case of turbulent flow inside a parallel plate channel, the effect of axial heat conduction within the fluid was only studied by Faggiani and Gori [13]. They solved numerically the energy equation for a duct where one wall was subjected to a constant heat flux while the second wall was insulated.

Nearly all of the above-mentioned investigations only considered a heating section which is semi-infinite in length. Hennecke [3] was one of the few who calculated the temperature distribution at the end of a long heated zone for laminar pipe flow. However, he only investigated one length of the heated zone and did not show the effect of changing length of the heated section on the temperature field in the flow. Additionally no analytical study is known in the literature which deals with the effect of axial heat conduction in a parallel plate channel with a piecewise heated wall.

The purpose of the present paper is to derive an exact analytical solution for the extended Graetz problem with

piecewise constant heat flux at the wall. The solution will be given for laminar and turbulent internal flows with low Peclet numbers inside a parallel plate channel as well as inside a circular pipe. By using the solution method according to Papoutsakis et al. [6] and Weigand [12] it is possible to derive analytical solutions for the extended Graetz problem which are computationally as simple and efficient as the solution for the parabolic problem. Additionally, the solutions presented here are used to show the effect of a finite heated length on the distribution of the Nusselt number and the temperature field. This case elucidates that axial heat conduction effects can also be of interest for larger Peclet numbers, if the heated section is smaller in size.

2. Analysis

Fig. 1 shows the geometrical configuration and the coordinate system. It is assumed that the flow enters the duct with a fully developed laminar or turbulent velocity profile and with a uniform temperature distribution T_0 for $x \to -\infty$. For $0 < x < x_1$ the duct is uniformly heated by applying the constant heat flux $\dot{q}_w$ to the wall. The characteristic length L, indicated in Fig. 1, denotes half of the channel height h for the flow in a parallel plate channel or the radius R for the flow in a circular pipe. Under the assumptions of an incompressible flow with constant physical properties, negligible viscous and turbulent energy dissipation and hydrodynamically fully developed flow, the energy equation is given by

$$\rho c_p u \frac{\partial T}{\partial x} = \frac{\partial}{\partial x}\left[\left(k + \rho c_p \varepsilon_{hx}\right)\frac{\partial T}{\partial x}\right] + \frac{1}{r^k}\frac{\partial}{\partial n}\left[r^k\left(k + \rho c_p \varepsilon_{hn}\right)\frac{\partial T}{\partial n}\right] \tag{1}$$

with the boundary conditions

$$\begin{aligned} &n = 0: \quad \partial T/\partial n = 0,\\ &n = L: \quad x < 0,\ x \geqslant x_1: \quad \partial T/\partial n = 0,\\ &\qquad 0 \leqslant x < x_1: \quad \partial T/\partial n = \dot{q}_w/k,\\ &\lim_{x\to-\infty} T = T_0. \end{aligned} \tag{2}$$

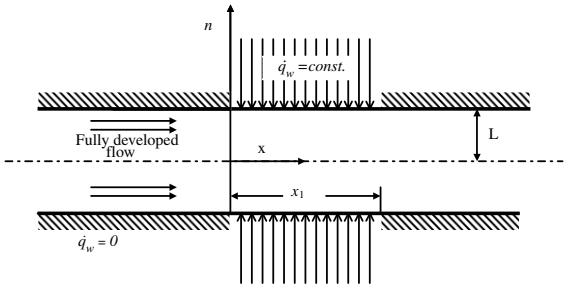

Fig. 1. Geometrical configuration and coordinate system.

The index k, which appears in Eq. (1), is equal to 0 for a planar duct and equal to 1 for a circular pipe. For $k = 1$ the coordinate n is equal to r (circular pipe). The hydrodynamically fully developed velocity distribution u, which appears in Eq. (1), has been calculated from the momentum equation by using the well-known Nikuradse mixing length distribution with the van Driest damping factor. The reader is referred to [12] for more details.

By introducing the following dimensionless quantities,

$$\begin{aligned} &\theta = \frac{T - T_0}{\dot{q}_w L/k}, \quad \tilde{x} = \frac{x}{L}\frac{1}{Pe_L}, \quad \tilde{u} = \frac{u}{\bar{u}_0}, \quad \tilde{n} = \frac{n}{L}, \quad \tilde{r} = \frac{r}{L},\\ &Pe_L = Re_L Pr, \quad Re_L = \frac{\bar{u}_0 L}{\nu}, \quad Pr = \frac{\nu}{a},\\ &\tilde{\varepsilon}_m = \frac{\varepsilon_m}{\nu}, \quad Pr_t = \frac{\varepsilon_m}{\varepsilon_{hn}} \end{aligned} \tag{3}$$

into Eqs. (1) and (2) the energy equation can be cast into the following form:

$$\tilde{u}\frac{\partial\theta}{\partial\tilde{x}} = \frac{1}{Pe_L^2}\frac{\partial}{\partial\tilde{x}}\left[a_1\frac{\partial\theta}{\partial\tilde{x}}\right] + \frac{1}{\tilde{r}^k}\frac{\partial}{\partial\tilde{n}}\left[\tilde{r}^k a_2\frac{\partial\theta}{\partial\tilde{n}}\right] \tag{4}$$

with the boundary conditions

$$\begin{aligned} &\tilde{x} \to -\infty: \quad \theta = 0,\\ &\tilde{n} = 0: \quad \frac{\partial\theta}{\partial\tilde{n}} = 0,\\ &\tilde{n} = 1: \quad 0 \leqslant \tilde{x} < \tilde{x}_1: \quad \frac{\partial\theta}{\partial\tilde{n}} = 1,\\ &\tilde{x} < 0, \quad \tilde{x} \geqslant \tilde{x}_1: \quad \frac{\partial\theta}{\partial\tilde{n}} = 0. \end{aligned} \tag{5}$$

The functions $a_1(\tilde{n})$ and $a_2(\tilde{n})$ are given by

$$a_1(\tilde{n}) = 1 + \frac{Pr}{Pr_t}\tilde{\varepsilon}_m\left(\frac{\varepsilon_{hx}}{\varepsilon_{hn}}\right), \quad a_2(\tilde{n}) = 1 + \frac{Pr}{Pr_t}\tilde{\varepsilon}_m. \tag{6}$$

In the following solution process for Eq. (4) no assumptions are required about the functions $a_1(\tilde{n})$ and $a_2(\tilde{n})$. The solution holds for arbitrary functions $a_1(\tilde{n}) \geqslant 1$ and $a_2(\tilde{n}) \geqslant 1$. This condition is obviously satisfied by Eq. (6). The turbulent Prandtl number as well as the ratio $\varepsilon_{hx}/\varepsilon_{hn}$ which were used for the calculations will be specified later.

Papoutsakis et al. [5] showed that Eq. (4), together with the boundary conditions according to Eq. (5), can be solved for laminar pipe flow ($a_1 = a_2 = 1$) by decomposing the elliptic partial differential equation into a pair of first-order partial differential equations. Weigand [12] showed how the method of Papoutsakis et al. [6] can be adapted for solving the extended turbulent Graetz problem for constant wall temperature. The ensuing procedure for solving Eqs. (4) and (5) follows [5,12].

Let us define a function $\Sigma(\tilde{x},\tilde{n})$ which represents the axial energy flow through a cross-sectional area of the height $\tilde{n}$ by

$$\Sigma = \int_0^{\tilde{n}} \left[\tilde{u}\theta - \frac{1}{Pe_L^2} a_1(\bar{n}) \frac{\partial\theta}{\partial\tilde{x}}\right] \tilde{r}^k \,\mathrm{d}\bar{n}. \tag{7}$$

Introducing Σ, defined by Eq. (7), into the energy equation (4) results in the following system of partial differential equations:

$$\frac{\partial}{\partial\tilde{x}} \vec{F}(\tilde{x},\tilde{n}) = \underset{\sim}{L}\vec{F}(\tilde{x},\tilde{n}) \tag{8}$$

with the two component vector $\vec{F}$ and the operator $\underset{\sim}{L}$ given by

$$\vec{F} = \begin{bmatrix} \theta(\tilde{x},\tilde{n}) \\ \Sigma(\tilde{x},\tilde{n}) \end{bmatrix}, \quad \underset{\sim}{L} = \begin{bmatrix} \frac{Pe_L\tilde{u}}{a_1(\tilde{n})} & -\frac{Pe_L^2}{\tilde{r}^k a_1(\tilde{n})}\frac{\partial}{\partial\tilde{n}} \\ \tilde{r}^k a_2(\tilde{n})\frac{\partial}{\partial\tilde{n}} & 0 \end{bmatrix}. \tag{9}$$

The boundary conditions belonging to $\Sigma(\tilde{x},\tilde{n})$ can be derived from Eqs. (5) and (7):

$$\lim_{\tilde{x}\to-\infty} \Sigma = 0, \quad \tilde{n} = 0: \ \Sigma = 0,$$

$$\tilde{n} = 1: \quad \Sigma = \begin{cases} 0, & -\infty < \tilde{x} \leqslant 0, \\ \tilde{x}, & 0 < \tilde{x} \leqslant \tilde{x}_1, \\ \tilde{x}_1, & \tilde{x}_1 < \tilde{x} \leqslant \infty. \end{cases} \tag{10}$$

Following the work of Papoutsakis et al. [5] and Weigand [12] it can be shown that the operator $\underset{\sim}{L}$ gives rise to a self-adjoint problem even though the original convective diffusion operator is non-selfadjoint. This fact is of course dependent on the sort of inner product between two vectors which is used. If we define an inner product between two vectors

$$\vec{\Phi} = \begin{bmatrix} \Phi_1(\tilde{n}) \\ \Phi_2(\tilde{n}) \end{bmatrix}, \quad \vec{\Lambda} = \begin{bmatrix} \Lambda_1(\tilde{n}) \\ \Lambda_2(\tilde{n}) \end{bmatrix} \tag{11}$$

according to Weigand [12] as

$$\left\langle \vec{\Phi}, \vec{\Lambda} \right\rangle = \int_0^1 \left[\frac{a_1(\tilde{n})\tilde{r}^k}{Pe_L^2} \Phi_1(\tilde{n})\Lambda_1(\tilde{n}) + \frac{1}{a_2(\tilde{n})\tilde{r}^k} \Phi_2(\tilde{n})\Lambda_2(\tilde{n}) \right] \mathrm{d}\tilde{n} \tag{12}$$

and the following domain for $\underset{\sim}{L}$

$$D(\underset{\sim}{L}) = \left\{ \vec{\Phi} \in H : (\exists \underset{\sim}{L}\vec{\Phi} \in H), \ \Phi_2(1) = \Phi_2(0) = 0 \right\}, \tag{13}$$

then it can be shown that L is a symmetric operator in the Hilbert space H of interest (this means that $\langle \vec{\Phi}, \underset{\sim}{L}\vec{\Lambda} \rangle = \langle \underset{\sim}{L}\vec{\Phi}, \vec{\Lambda} \rangle$). For a detailed explanation see Weigand [12]. Thus the self-adjoint eigenvalue problem associated with Eq. (8) is given by

$$\underset{\sim}{L}\vec{\Phi}_j = \lambda_j \vec{\Phi}_j, \tag{14}$$

where $\vec{\Phi}_j$ is the eigenvector corresponding to the eigenvalue λ_j. Using the definition of L, the eigenvalue problem, Eq. (14), can be rewritten as

$$Pe_L^2 \left[\frac{\tilde{u}}{a_1(\tilde{n})} \Phi_{j1} - \frac{1}{\tilde{r}^k a_1(\tilde{n})} \Phi'_{j2} \right] = \lambda_j \Phi_{j1}, \tag{15}$$

$$\tilde{r}^k a_2(\tilde{n}) \Phi'_{j1} = \lambda_j \Phi_{j2}. \tag{16}$$

Eliminating Φ'_{j2} from Eq. (15) results in the following eigenvalue problem for Φ_{j1}:

$$\left[\tilde{r}^k a_2(\tilde{n})\Phi'_{j1}\right]' + \tilde{r}^k \left[\frac{\lambda_j a_1(\tilde{n})}{Pe_L^2} - \tilde{u} \right] \lambda_j \Phi_{j1} = 0. \tag{17}$$

Eq. (17) has to be solved with the following boundary conditions:

$$\Phi'_{j1}(0) = 0, \quad \Phi'_{j1}(1) = 0. \tag{18}$$

Additionally an arbitrary normalising condition

$$\Phi_{j1}(0) = 1 \tag{19}$$

has been used. Eq. (17) possesses both positive and negative eigenvalues. This is because the operator L is neither positive nor negative definite. All λ_j are real because they are in fact the eigenvalues of a self-adjoint problem. For $a_1(\tilde{n})/Pe_L^2 \to 0$ the eigenvalue problem given by Eq. (17) reduces to the parabolic Graetz problem in turbulent flow with no effect of axial heat conduction. For $a_1 = a_2 = 1$ and a laminar velocity profile for $\tilde{u}$ the eigenvalue problem reduces to the extended Graetz problem for laminar flow. Because the two sets of eigenvectors constitute an orthonormal basis in H (see also [12]) an arbitrary vector $\vec{F}$ can be expanded in terms of eigenfunctions in the following way:

$$\vec{f} = \sum_{j=1}^{\infty} \frac{\left\langle \vec{f}, \vec{\Phi}_j \right\rangle}{\left\| \vec{\Phi}_j \right\|^2} \vec{\Phi}_j(\tilde{n}) = \sum_{j=1}^{\infty} \frac{\left\langle \vec{f}, \vec{\Phi}_j^+ \right\rangle}{\left\| \vec{\Phi}_j^+ \right\|^2} \vec{\Phi}_j^+(\tilde{n}) + \sum_{j=1}^{\infty} \frac{\left\langle \vec{f}, \vec{\Phi}_j^- \right\rangle}{\left\| \vec{\Phi}_j^- \right\|^2} \vec{\Phi}_j^-(\tilde{n}) \tag{20}$$

with the vector norm $\|\vec{\Phi}_j\|^2 = \langle \vec{\Phi}_j, \vec{\Phi}_j \rangle$.

Now let us reconsider the solution of Eq. (4). The solution of the problem $\vec{F}(\tilde{x},\tilde{n})$ will be obtained in the form of a series according to Eq. (20). Therefore, the inner product appearing in the expansion coefficients in Eq. (20) must be determined. By using Eq. (12) and recalling that $\underset{\sim}{L}$ is a symmetric operator in D, one obtains

$$\left\langle \underset{\sim}{L}\vec{F}, \vec{\Phi}_j \right\rangle = \left\langle \vec{F}, \underset{\sim}{L}\vec{\Phi}_j \right\rangle - \Phi_{j1}(1)\Sigma(\tilde{x},1). \tag{21}$$

Now applying the inner product, defined in Eq. (12), to both sides of Eq. (14) and using this equation, one derives from Eq. (21)

$$\left\langle \underset{\sim}{L}\vec{F}, \vec{\Phi}_j \right\rangle = \lambda_j \left\langle \vec{F}, \vec{\Phi}_j \right\rangle - \Phi_{j1}(1)\Sigma(\tilde{x}, 1). \tag{22}$$

Taking the inner product of both sides of Eq. (8) with $\vec{\Phi}_j$ and using Eq. (22) one finally obtains

$$\frac{\partial}{\partial \tilde{x}} \left\langle \vec{F}, \vec{\Phi}_j \right\rangle = \lambda_j \left\langle \vec{F}, \vec{\Phi}_j \right\rangle - \Phi_{j1}(1)\Sigma(\tilde{x}, 1), \tag{23}$$

where $\Sigma(x, 1)$ is given by the boundary conditions according to Eq. (10). Eq. (23) can be solved separately for positive and negative eigenvalues. This results in

$$\left\langle \vec{F}, \vec{\Phi}_j^- \right\rangle = -\Phi_{j1}^-(1) \int_{-\infty}^{\tilde{x}} \Sigma(\tilde{x}, 1) \exp(\lambda_j^-(\tilde{x} - \bar{x}))\, \mathrm{d}\bar{x} \tag{24}$$

$$\left\langle \vec{F}, \vec{\Phi}_j^+ \right\rangle = \Phi_{j1}^+(1) \int_{\tilde{x}}^{\infty} \Sigma(\tilde{x}, 1) \exp(\lambda_j^+(\tilde{x} - \bar{x}))\, \mathrm{d}\bar{x}. \tag{25}$$

After evaluating the integrals in Eqs. (24) and (25), the following results for $\theta(\tilde{x}, \tilde{n})$, which is the first vector component of $\vec{F}(\tilde{x}, \tilde{n})$, can be derived.

$\tilde{x} < 0$:

$$\theta(\tilde{x}, \tilde{n}) = \sum_{j=1}^{\infty} \frac{\Phi_{j1}^+(1)}{\left\|\vec{\Phi}_j^+\right\|^2} \frac{\exp\left(\lambda_j^+ \tilde{x}\right)}{\lambda_j^{+2}} \times \left[1 - \exp\left(-\lambda_j^+ \tilde{x}_1\right)\right] \Phi_{j1}^+(\tilde{n}), \tag{26}$$

$0 < \tilde{x} < \tilde{x}_1$:

$$\begin{aligned} \theta(\tilde{x}, \tilde{n}) = {} & \sum_{j=1}^{\infty} \frac{\Phi_{j1}(1)}{\lambda_j^2 \left\|\vec{\Phi}_j\right\|^2} \Phi_{i1}(\tilde{n}) + \tilde{x} \sum_{j=1}^{\infty} \frac{\Phi_{j1}(1)}{\lambda_j \left\|\vec{\Phi}_j\right\|^2} \Phi_{j1}(\tilde{n}) \\ & - \sum_{j=1}^{\infty} \frac{\Phi_{j1}^-(1)}{\left\|\vec{\Phi}_j^-\right\|^2} \frac{\exp\left(\lambda_j^- \tilde{x}\right)}{\lambda_j^{-2}} \Phi_{j1}^-(\tilde{n}) \\ & - \sum_{j=1}^{\infty} \frac{\Phi_{j1}^+(1)}{\left\|\vec{\Phi}_j^+\right\|^2} \frac{\exp\left(\lambda_j^+ (\tilde{x} - \tilde{x}_1)\right)}{\lambda_j^{+2}} \Phi_{j1}^+(\tilde{n}), \end{aligned} \tag{27}$$

$\tilde{x} > \tilde{x}_1$:

$$\begin{aligned} \theta(\tilde{x}, \tilde{n}) = {} & \sum_{j=1}^{\infty} \frac{\Phi_{j1}^-(1)}{\lambda_j^{-2} \left\|\vec{\Phi}_j^-\right\|^2} \exp\left(\lambda_j^-(\tilde{x} - \tilde{x}_1)\right) \Phi_{j1}^-(\tilde{n}) \\ & + \tilde{x}_1 \sum_{j=1}^{\infty} \frac{\Phi_{j1}(1)}{\lambda_j \left\|\vec{\Phi}_j\right\|^2} \Phi_{j1}(\tilde{n}) \\ & - \sum_{i=1}^{\infty} \frac{\Phi_{j1}^-(1)}{\left\|\vec{\Phi}_j^-\right\|^2} \frac{\exp\left(\lambda_j^- \tilde{x}\right)}{\lambda_j^{-2}} \Phi_{j1}^-(\tilde{n}). \end{aligned} \tag{28}$$

The temperature distribution given above contains for $0 < \tilde{x} < \tilde{x}_1$ both negative and positive eigenfunctions. The expressions for the temperature field can be further simplified by replacing the two sums

$$\begin{aligned} & \sum_{j=1}^{\infty} \frac{\Phi_{j1}(1)}{\lambda_j^2 \left\|\vec{\Phi}_j\right\|^2} \Phi_{i1}\left(\tilde{n}\right), \\ & \sum_{j=1}^{\infty} \frac{\Phi_{j1}(1)}{\lambda_j \left\|\vec{\Phi}_j\right\|^2} \Phi_{j1}\left(\tilde{n}\right) \end{aligned} \tag{29}$$

by analytical functions (see Appendix A). One finally obtains:

$\tilde{x} < 0$:

$$\theta\left(\tilde{x}, \tilde{n}\right) = \sum_{j=1}^{\infty} A_j^+ \Phi_{j1}^+\left(\tilde{n}\right) \left[1 - \exp\left(-\lambda_j^+ \tilde{x}_1\right)\right] \times \exp\left(\lambda_j^+ \tilde{x}\right), \tag{30}$$

$0 < \tilde{x} < \tilde{x}_1$:

$$\begin{aligned} \theta\left(\tilde{x}, \tilde{n}\right) = {} & \Psi\left(\tilde{n}\right) + (k+1)\tilde{x} - \sum_{j=1}^{\infty} A_j^- \Phi_{j1}^-\left(\tilde{n}\right) \exp\left(\lambda_j^- \tilde{x}\right) \\ & - \sum_{j=1}^{\infty} A_j^+ \Phi_{j1}^+\left(\tilde{n}\right) \exp\left(\lambda_j^+\left(\tilde{x} - \tilde{x}_1\right)\right). \end{aligned} \tag{31}$$

$\tilde{x} > \tilde{x}_1$:

$$\theta\left(\tilde{x}, \tilde{n}\right) = (k+1)\tilde{x}_1 + \sum_{j=1}^{\infty} A_j^- \Phi_{j1}^-\left(\tilde{n}\right) \times \left[\exp\left(-\lambda_j^- \tilde{x}_1\right) - 1\right] \exp\left(\lambda_j^- \tilde{x}\right) \tag{32}$$

with the function $\Psi(\tilde{n})$ given by

$$\begin{aligned} \Psi\left(\tilde{n}\right) &= \int_0^{\tilde{n}} \frac{k+1}{\tilde{r}^k a_2\left(\bar{n}\right)} \int_0^{\tilde{n}} \tilde{u}(s) \tilde{r}^k \, \mathrm{d}s \, \mathrm{d}\bar{n} + C_2 \\ &= \bar{\Psi}\left(\tilde{n}\right) + C_2, \end{aligned} \tag{33}$$

where

$$C_2 = \frac{(k+1)^2}{Pe_L^2} \int_0^1 \tilde{r}^k a_1\left(\tilde{n}\right) \mathrm{d}\tilde{n} - (k+1) \times \int_0^1 \tilde{r}^k \tilde{u}(\tilde{n}) \bar{\Psi}(\tilde{n}) \, \mathrm{d}\tilde{n}. \tag{34}$$

The coefficients A_j are defined by

$$A_j = \frac{\Phi_{j1}(1)}{\lambda_j^2 \left\|\vec{\Phi}_j\right\|^2} = -\frac{1}{\lambda_j^2 (\mathrm{d}/\mathrm{d}\lambda)(\Phi_{j1}'/\lambda)_{\lambda=\lambda_j}}. \tag{35}$$

After the temperature field is known, the bulk temperature

$$T_b = \int_0^1 uTr^k \,dn \Big/ \int_0^1 ur^k \,dn \tag{36}$$

and the Nusselt number

$$Nu_D = -D\left(\frac{\partial T}{\partial n}\right)_{n=L} \Big/ (T_b - T_w) \tag{37}$$

can be calculated. Introducing the predicted temperature field in the flow into the above expressions for T_b and Nu_D, one obtains:

$\tilde{x} < 0$:

$$\theta_b(\tilde{x}) = (k+1)\sum_{i=1}^{\infty} A_j^+ \left[1 - \exp\left(-\lambda_j^+ \tilde{x}_1\right)\right] \exp\left(\lambda_j^+ \tilde{x}\right) \times \int_0^1 \tilde{u}\tilde{r}^k \Phi_{j1}^+\left(\tilde{n}\right) d\tilde{n}. \tag{38}$$

$0 < \tilde{x} < \tilde{x}_1$:

$$\theta_b(\tilde{x}) = \frac{(k+1)^2}{Pe_L^2} \int_0^1 \tilde{r}^k a_1\left(\tilde{n}\right) d\tilde{n} + (k+1)\tilde{x} - (k+1) \times \sum_{j=1}^{\infty} A_j^- \exp\left(\lambda_j^- \tilde{x}\right) \int_0^1 \tilde{u}\tilde{r}^k \Phi_{j1}^-\left(\tilde{n}\right) d\tilde{n} - (k+1) \times \sum_{j=1}^{\infty} A_j^+ \exp\left(\lambda_j^+\left(\tilde{x} - \tilde{x}_1\right)\right) \int_0^1 \tilde{u}\tilde{r}^k \Phi_{j1}^+(\tilde{n})\, d\tilde{n}. \tag{39}$$

$\tilde{x} > \tilde{x}_1$:

$$\theta_b(\tilde{x}) = (k+1)\tilde{x}_1 - (k+1)\sum_{j=1}^{\infty} A_j^- \left[\exp\left(-\lambda_j^- \tilde{x}_1\right) - 1\right] \times \exp\left(\lambda_j^- \tilde{x}\right) \int_0^1 \tilde{u}\tilde{r}^k \Phi_{j1}^-(\tilde{n})\, d\tilde{n}. \tag{40}$$

The Nusselt number is zero for $\tilde{x} < 0$ and for $\tilde{x} > \tilde{x}_1$ because there is zero heat flux at the wall. For $0 < \tilde{x} < \tilde{x}_1$ the Nusselt number is given by:

$$Nu_D = -\frac{4}{(k+1)} \left\{ \frac{(k+1)^2}{Pe_L^2} \int_0^1 \tilde{r}^k a_1(\tilde{n})\, d\tilde{n} - \Psi(1) - \sum_{j=1}^{\infty} A_j^- \exp(\lambda_j^- \tilde{x}) \times \left[(k+1)\int_0^1 \tilde{u}\tilde{r}^k \Phi_{j1}^-(\tilde{n})\, d\tilde{n} - \Phi_{j1}^-(1)\right] - \sum_{j=1}^{\infty} A_j^+ \exp(\lambda_j^+(\tilde{x} - \tilde{x}_1)) \times \left[(k-1)\int_0^1 \tilde{u}\tilde{r}^k \Phi_{j1}^+(\tilde{n})\, d\tilde{n} - \Phi_{j1}^+(1)\right] \right\}^{-1}. \tag{41}$$

3. Results and discussion

In order to obtain a solution of the energy equation (4), the ratio $(\varepsilon_{hx}/\varepsilon_{hn})$ of the eddy diffusivity must be specified. In the following calculations this ratio is set to one. This assumption has been made previously by Lee [10] and by Chieng and Launder [14]. Additionally, the turbulent Prandtl number has to be specified. For the case of liquid metal flows there is a huge variety of different models [15]. For the present study, the model of Weigand et al. [16]

$$Pr_t = 1 \Big/ \left\{ \frac{1}{2Pr_{t\infty}} + CPe_t\sqrt{\frac{1}{Pr_{t\infty}}} + (CPe_t)^2 \times \left[1 - \exp\left(-\frac{1}{CPe_t\sqrt{Pr_{t\infty}}}\right)\right]\right\}, \tag{42}$$

$$Pe_t = Pr\frac{\varepsilon_m}{\nu}, \quad Pr_{t\infty} = 0.85 + \frac{100}{PrRe^{0.888}}, \quad C = 0.3 \tag{43}$$

has been used, because the model has proved to produce reliable results for predicted Nusselt numbers for liquid metal flows [16]. Nevertheless, it should be noted that the analysis presented in the previous chapter is more general and can be used with any turbulent Prandtl number concept and with arbitrary functions for $a_1(\tilde{n})$ and $a_2(\tilde{n})$.

3.1. Numerical procedure and accuracy of the predictions

The evaluation of the sums for the temperature distribution and for the Nusselt number require that the eigenfunctions and the eigenvalues are known. For this analytical study these quantities have been calculated numerically by solving the eigenvalue problem, given by Eqs. (17)–(19) with the help of a four stage Runge–Kutta method. By comparing the calculated eigenvalues and constants for the special case of laminar pipe flow ($a_1 = a_2 = 1,\ \tilde{u} = 2(1 - \tilde{n}^2)$) with values given in [5,6] it could be seen that the relative error is of the order of 10^{-6}. Additionally care has been taken by evaluating the sum expressions for the temperature field and the Nusselt number, so that the number of eigenvalues and eigenfunctions has been high enough. Normally 100 eigenvalues and eigenfunctions and about 1000 grid points in n-direction guaranteed very precise results.

3.2. Circular pipe

3.2.1. Laminar flow

For the case of laminar pipe flow ($a_1 = a_2 = 1$, $\tilde{u} = 2(1 - \tilde{n}^2)$), the results can be compared with predictions available in the literature. Fig. 2 shows the distribution of the Nusselt number for a semi-infinite heating length. The results are compared to several nu-

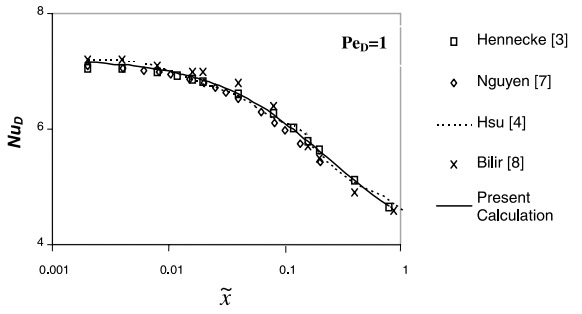

Fig. 2. Variation of the local Nusselt number in the thermal entry region of a circular pipe for laminar flow.

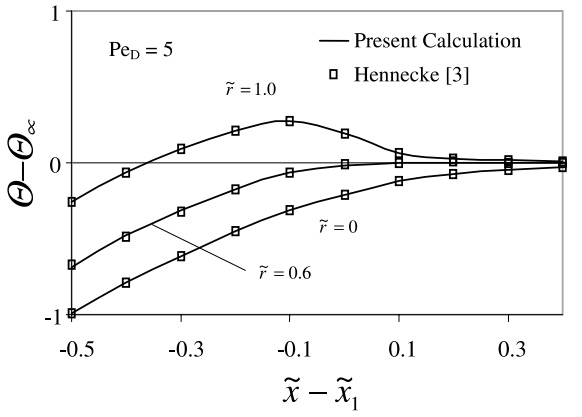

Fig. 3. Temperature distribution near the end of the heating section for a circular pipe ($Pe_D = 5$).

merical calculations by Hennecke [3], Nguyen [7], Bilir [8] and with the analytical prediction by Hsu [4]. It can be seen from Fig. 2 that the present analytical solution agrees very well with the other results.

As mentioned before, Hennecke [3] was one of the few who investigated also the distribution of the temperature field at the end of the heated section. He showed results for one fixed length of a long heated section. Fig. 3 shows temperature profiles for three different values of the radial coordinate at the end of the heating zone. The agreement between Henneckes numerical predictions and the analytical solution is excellent. Fig. 3 shows also that the wall temperature has an overshoot near the end of the heating section, before it attains the outlet temperature. This behaviour can also been seen more clearly in Fig. 4. In this figure, the centreline temperature as well as the wall temperature are shown for two different values of the Peclet number and two different length of the heating section ($\tilde{x}_1 = 0.7$ and $\tilde{x}_1 = 1.3$). For a Peclet number $Pe_D = 10$ it can be seen that the wall temperature for $\tilde{x}_1 = 1.3$ adopts a linear shape in the middle of the heating section. This indicates a nearly fully developed behaviour of the heat transfer in this region. However, near the end of the heating section, a strong change in the wall temperature can be observed. Of course, this behaviour can only be captured if the fully elliptic energy equation is solved. For the smaller Peclet number ($Pe_D = 2$), the temperature distribution within the whole heating section is dominated by elliptic effects. The wall temperature, for example, never attains a linear shape. Fig. 5 shows the distribution of the Nusselt number near the end of the long heated zone for two different Peclet numbers. The present analytical calculation is compared with the numerical calculation by Hennecke [3] and good agreement is found. Fig. 6 shows the distribution of the Nusselt number for a short heated section with a length of $\tilde{x}_1 = 0.1$ for different values of the Peclet number. It can be seen that the Nusselt number decreases with increasing axial distance from the start of the heating zone up to a point where a nearly constant value of the Nusselt number is reached. When the end of the heating section is approached, the value of the Nusselt number rises again. This behaviour is caused by axial heat conduction effects within the flow. Near the start and the end of the heating zone the fluid temperature is changed by axial heat conduction within the flow causing lower mean fluid temperature in the flow as in the case of the parabolic problem. This results in increasing values of the Nusselt number in this areas. With increasing values of the Peclet number, the shape of the Nusselt number approaches the one for the parabolic problem. The increase in Nusselt number at the end of the heated section is therefore not so much pronounced. Fig. 6 elucidates therefore the significance of axial heat conduction effects in the flow for shorter heated zones.

3.2.2. Turbulent flow

Table 1 shows positive and negative eigenvalues and constants for $Pr = 0.001$ and various values of Reynolds number. From the table it can be seen that the positive eigenvalues for $\tilde{x} < 0$ increase dramatically with increasing values of Reynolds number, indicating the vanishing effect of axial heat conduction within the fluid. As in the case of laminar internal flow, we consider two different cases for turbulent internal flow. The first one, is a semi-infinite heating section ($\tilde{x} > 0$) which has also been considered by Lee [10] by using the method of Hsu [4]. For the case of fully developed flow, Fig. 7 shows a comparison between experimental data of Fuchs [17] for liquid Na ($Pr = 0.007$) and the present calculations. As it can be seen from the figure, the agreement between the theoretical and experimental data is very good. Fig. 8 shows the distribution of the local Nusselt number for $Pr = 0.001$ for various values of Peclet number. It can be seen that the Nusselt number for the fully developed flow increases with Peclet number. Fig. 9 shows the distribution of the bulk

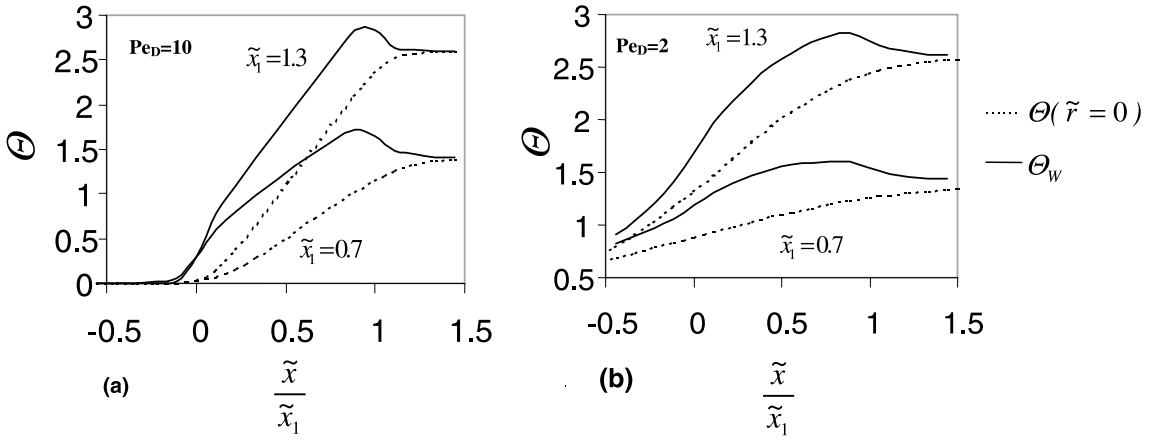

Fig. 4. Centreline and wall temperature distribution in the heating section of a circular pipe.

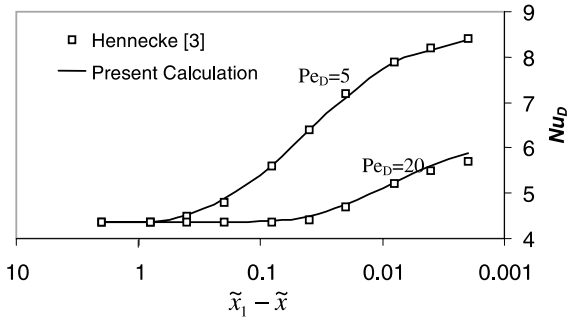

Fig. 5. Nusselt number near the end of the heating section in a circular pipe.

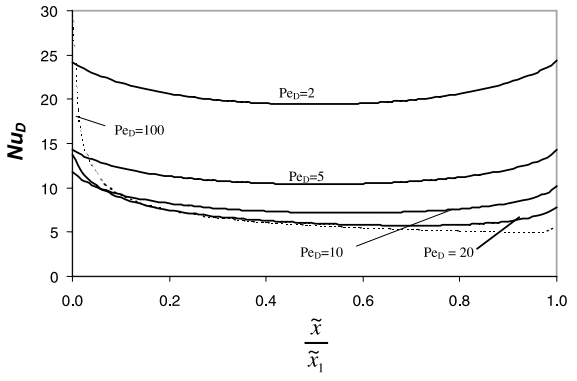

Fig. 6. Distribution of the local Nusselt number within the heating section of a circular pipe.

temperature for a semi-infinite heated section for different values of Peclet number and $Pr = 0.001$. This figure shows very clearly the effect of axial heat conduction within the flow. Axial conduction effects within the flow change the distribution of the bulk temperature for lower Peclet numbers and result in an increased value of the bulk temperature at $x = 0$. With increasing Peclet number this effect reduces and the bulk temperature shows a linear distribution starting very closely to $x = 0$ with a value of approximately zero.

Let us now consider the case of a finite heated section: Fig. 10 shows the distribution of the Nusselt number for a short heated section of $\tilde{x}_1 = 0.1$ and a Prandtl number of $Pr = 0.001$. By comparing Fig. 10 with the comparable situation for laminar flow (Fig. 6), it can be seen that the turbulent flow results in a higher Nusselt number for the same Peclet number. Additionally it can be noticed that also for turbulent flow the same shape of the curves occur as for laminar flow, with the difference that the change in the mean Nusselt number with increasing Peclet numbers is more pronounced for the laminar flow. This is caused by turbulent mixing in the flow, resulting in more uniform velocity and temperature profiles.

Fig. 11 shows a comparison between a calculation considering and one neglecting axial heat conduction within the flow. From Fig. 11, it can be seen that the relative error, which is made by neglecting the axial heat conduction effects in the flow can be quite large. Of course, the largest error always appears at the start and the end of the heated section. Fig. 11 shows also the relative error for a larger Peclet number of 10. It is noticeable, that the deviation between both calculations is in this case only significant near the start and the end of the heating section.

3.3. Parallel plates

3.3.1. Laminar flow

The flow index k in the preceding equations must be set to zero for the calculation of the heat transfer in a

Table 1
Eigenvalues and constants for various Reynolds numbers and $Pr = 0.001$ (circular pipe with turbulent flow)

Re	j	λ_j^-	A_j^-	λ_j^+	A_j^+
5000	1	−6.8028E+0	−2.3412E−1	6.1136E+0	2.9822E−1
	2	−1.4470E+1	8.3891E−2	1.3660E+1	−9.8091E−2
	3	−2.2238E+1	−4.5562E−2	2.1339E+1	5.0966E−2
	4	−3.0041E+1	2.9470E−2	2.9140E+1	−3.1758E−2
	5	−3.7862E+1	−2.0998E−2	3.6969E+1	2.2138E−2
	6	−4.5693E+1	1.5913E−2	4.4809E+1	−1.6552E−2
	7	−5.3530E+1	−1.2585E−2	5.2654E+1	1.2978E−2
	8	−6.1371E+1	1.0270E−2	6.0501E+1	−1.0528E−2
	9	−6.9214E+1	−8.5839E−3	6.8350E+1	8.7644E−3
	10	−7.7060E+1	7.3122E−3	7.6200E+1	−7.4440E−3
10,000	1	−1.0059E+1	−2.7799E−1	2.3675E+1	5.6338E−2
	2	−2.4181E+1	9.6515E−2	3.7596E+1	−5.0159E−2
	3	−3.9174E+1	−5.1052E−2	5.1350E+1	3.7686E−2
	4	−5.4474E+1	3.2438E−2	6.6342E+1	−2.6098E−2
	5	−6.9917E+1	−2.2826E−2	8.1681E+1	1.9121E−2
	6	−8.5439E+1	1.7138E−2	9.7164E+1	−1.4715E−2
	7	−1.0101E+2	−1.3457E−2	1.1272E+2	1.1757E−2
	8	−1.1661E+2	1.0919E−2	1.2832E+2	−9.6657E−3
	9	−1.3223E+2	−9.0834E−3	1.4395E+2	8.1264E−3
	10	−1.4787E+2	7.7068E−3	1.5959E+2	−6.9555E−3
15,000	1	−1.1654E+1	−3.0543E−1	5.1532E+1	1.4659E−2
	2	−3.0642E+1	1.0690E−1	7.4113E+1	−2.4560E−2
	3	−5.1979E+1	−5.5928E−2	9.1741E+1	2.7020E−2
	4	−7.4246E+1	3.5141E−2	1.1285E+2	−2.1127E−2
	5	−9.6964E+1	−2.4503E−2	1.3509E+2	1.6385E−2
	6	−1.1993E+2	1.8265E−2	1.5784E+2	−1.3028E−2
	7	−1.4305E+2	−1.4259E−2	1.8084E+2	0.0630E−2
	8	−1.6627E+2	1.1515E−2	2.0400E+2	−8.8682E−3
	9	−1.8956E+2	−9.5420E−3	2.2726E+2	7.5365E−3
	10	−2.1291E+2	8.0691E−3	2.5059E+2	−6.5039E−3

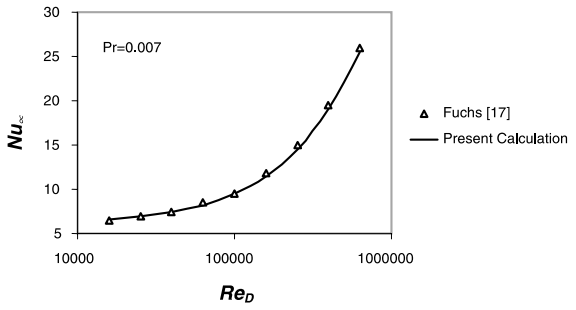

Fig. 7. Nusselt number for fully developed turbulent pipe flow as a function of the Reynolds number.

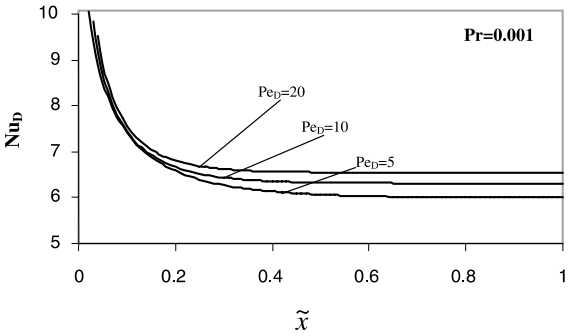

Fig. 8. Variation of the local Nusselt number in the thermal entry region for turbulent pipe flow.

parallel plate channel. Fig. 12 shows the development of the temperature profiles in the channel at different axial positions for $Pe_D = 5$. The influence of axial heat conduction within the flow, which causes changes in the temperature profiles for $x < 0$ is clearly visible. Fig. 13 shows the distribution of the local Nusselt number for a finite heated section for different values of the heating length $\tilde{x}_1$. It can be noticed that the mean value of the Nusselt number decreases with increasing length of the heating section because of the weaker influence of the axial heat conduction within the flow.

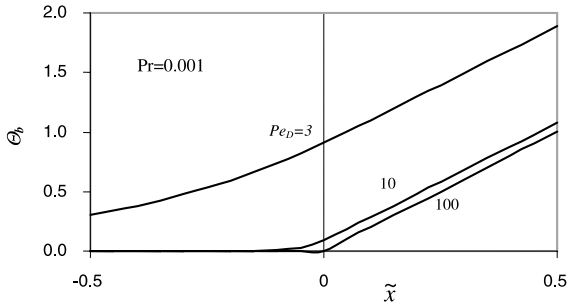

Fig. 9. Variation of the bulk temperature for turbulent pipe flow.

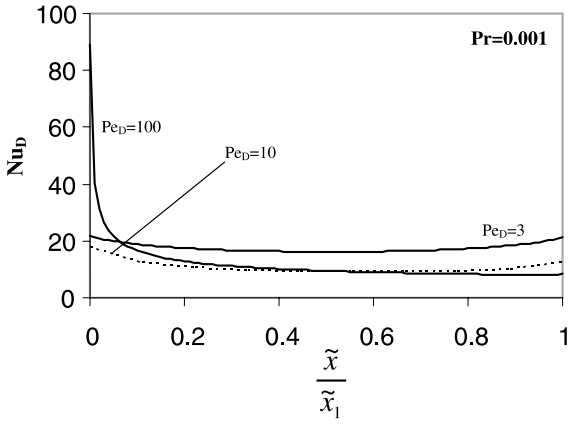

Fig. 10. Distribution of the local Nusselt number for a finite heating section with turbulent internal flow in a pipe.

3.3.2. Turbulent flow

Fig. 14 shows the distribution of the Nusselt number for a finite heated section. It can be seen that the heat transfer increases for a constant Peclet number with Reynolds number within the short heated section.

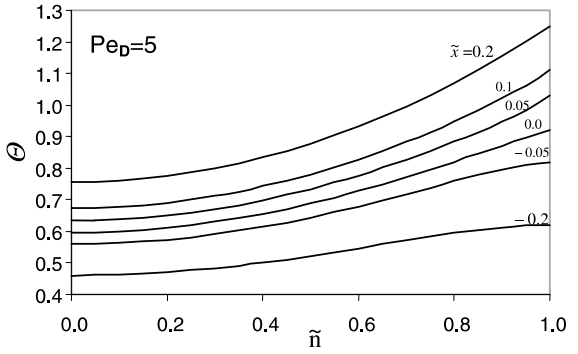

Fig. 12. Temperature distribution for laminar flow in a parallel plate channel.

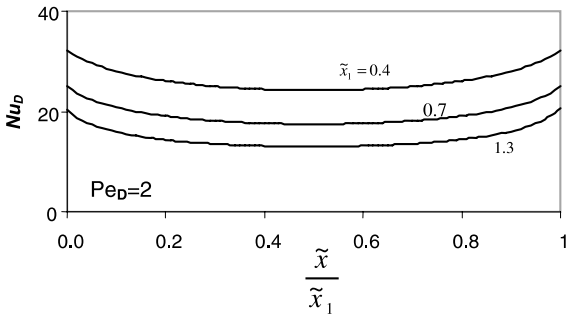

Fig. 13. Local Nusselt number for different length of the heating section in a parallel plate channel.

4. Conclusions

The present analytical study investigated the influence of axial heat conduction within the flow on heat transfer in a circular pipe and in a parallel plate channel with uniform heating at the wall. The two cases of semi-infinite and finite length of the heated sections have been

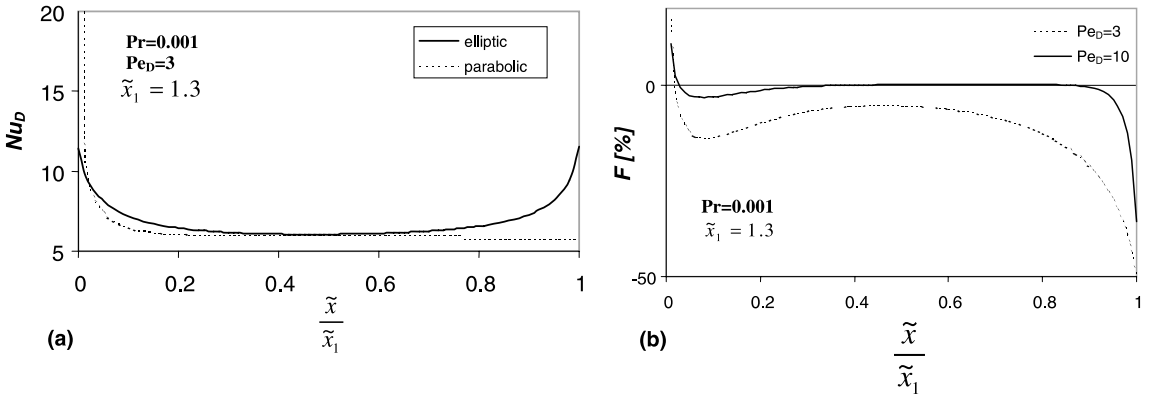

Fig. 11. Effect of axial heat conduction on the shape of the local Nusselt number for a circular pipe.

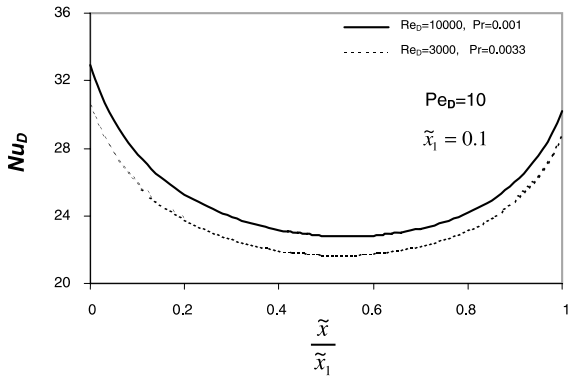

Fig. 14. Influence of the Reynolds number on the shape of the Nusselt number for a finite heated section in a parallel plate channel.

analysed. From the results obtained in the present investigation, we draw the following conclusions:

- The effect of axial heat conduction in the flow is important for low Peclet numbers. For a semi-infinite heated section the effect of axial heat conduction within the flow might be neglected for Peclet numbers larger than 20. For a finite length of the heated section the effect of axial heat conduction additionally depends on the length of the heated zone. Axial heat conduction effects will be important also for Peclet numbers larger than 100 if this zone is short.
- The obtained analytical results agree for pipe flow very well with several numerical calculations and with experimental results.
- By using a newly defined vector norm it is possible to obtain a self-adjoint eigenvalue problem for the extended turbulent Graetz problem even though the original convective diffusion operator is non-self-adjoint. Therefore, an entirely analytical solution to the extended turbulent Graetz problem with heat flux boundary conditions has been developed. The resulting equations for semi-infinite as well as finite heating length are as simple and efficient to compute as the related solutions of the parabolic problem.

Appendix A

This section shows how the temperature distribution, given by Eq. (27), can be further simplified by expressing two sums by analytical functions. The first sum is given by:

$$\sum_{i=1}^{\infty} \frac{\Phi_{i1}(1)\Phi_{i1}(\tilde{n})}{\lambda_i \left\| \vec{\Phi}_i \right\|^2}. \tag{A.1}$$

Expanding the vector $\vec{f} = [1,0]^{\mathrm{T}}$ into a series and using Eq. (15), one obtains

$$1 = \sum_{i=1}^{\infty} \frac{\Phi_{i1}(\tilde{n})}{\lambda_i \left\| \vec{\Phi}_i \right\|^2} \int_0^1 \tilde{u}\tilde{r}^k \Phi_{i1}(\tilde{n})\,\mathrm{d}\tilde{n}. \tag{A.2}$$

The integral, appearing in Eq. (A.2) can be rewritten by partial integration. By using also Eq. (16) this results finally in:

$$1 = \sum_{i=1}^{\infty} \frac{\Phi_{i1}(\tilde{n})}{\lambda_i \left\| \vec{\Phi}_i \right\|^2} \frac{\Phi_{i1}(1)}{k+1} - \sum_{i=1}^{\infty} \frac{\Phi_{i1}(\tilde{n})}{\lambda_i \left\| \vec{\Phi}_i \right\|^2} \times \int_0^1 \Phi_{i2}(\tilde{n}) h(\tilde{n})\,\mathrm{d}\tilde{n}, \tag{A.3}$$

$$h(\tilde{n}) = \frac{1}{\tilde{r}^k a_2(\tilde{n})} \int_0^{\tilde{n}} \tilde{u}\tilde{r}^k\,\mathrm{d}\bar{n}.$$

In order to obtain the expression for the investigated sum according to Eq. (A.1), the second term in Eq. (A.3) needs to be evaluated. Expanding the vector $\vec{f}_i = [0, h(\tilde{n})\tilde{r}^k a_2(\tilde{n})]^{\mathrm{T}}$ in a series and using the expression for the first vector component, one finally derives for the expression under investigation:

$$k+1 = \sum_{i=1}^{\infty} \frac{\Phi_{i1}(\tilde{n})\Phi_{i1}(1)}{\lambda_i \left\| \vec{\Phi}_i \right\|^2}. \tag{A.4}$$

Additionally we want to derive an analytical expression for the second sum:

$$\sum_{i=1}^{\infty} \frac{\Phi_{i1}(1)\Phi_{i1}(\tilde{n})}{\lambda_i^2 \left\| \vec{\Phi}_i \right\|^2}. \tag{A.5}$$

If we put $\tilde{x}_1 \to +\infty$ in Eq. (28), one obtains for the fully developed temperature distribution in the fluid:

$$\theta_\infty(\tilde{n}) = (k+1)\tilde{x} + \sum_{i=1}^{\infty} \frac{\Phi_{i1}(1)\Phi_{i1}(\tilde{n})}{\lambda_i^2 \left\| \vec{\Phi}_i \right\|^2} = (k+1)\tilde{x} + \Psi(\tilde{n}), \tag{A.6}$$

where $\Psi(\tilde{n})$ is not known. This function can be evaluated by inserting Eq. (A.6) into the energy equation (4) and solving the resulting ordinary differential equation for Ψ, one finally obtains

$$\Psi(\tilde{n}) = \int_0^{\tilde{n}} \frac{k+1}{\tilde{r}^k a_2(\tilde{n})} \int_0^{\bar{n}} \tilde{u}\tilde{r}^k\,\mathrm{d}s\,\mathrm{d}\bar{n} + C_2 = \bar{\Psi}(\tilde{n}) + C_2. \tag{A.7}$$

The constant C_2, which appears in Eq. (A.7) can be derived from a global energy balance. We might do that by evaluating Eq. (7) for the case of fully developed flow ($\tilde{x} \to +\infty$) and $\tilde{n} = 1$. By considering the boundary conditions according to Eq. (10), one obtains

$$\Sigma\left(\tilde{x},1\right) = \tilde{x} = \int_0^1 \left(\tilde{u}\Theta - \frac{1}{Pe_{\mathrm{L}}^2} a_1\left(\tilde{n}\right) \frac{\partial \Theta}{\partial \tilde{x}} \right) \tilde{r}^k\,\mathrm{d}\tilde{n}. \tag{A.8}$$

Inserting Eq. (A.6) into Eq. (A.8) results in

$$\int_0^1 \tilde{u}\tilde{r}^k \Psi(\tilde{n})\,\mathrm{d}\tilde{n} = \frac{(k+1)}{Pe_L^2}\int_0^1 a_1(\tilde{n})\tilde{r}^k\,\mathrm{d}\tilde{n}. \tag{A.9}$$

Comparing this equation with Eq. (A.7), one derives the following expression for the constant C_2:

$$C_2 = \frac{(k+1)^2}{Pe_L^2}\int_0^1 a_1(\tilde{n})\tilde{r}^k\,\mathrm{d}\tilde{n} - (k+1)\int_0^1 \tilde{u}\tilde{r}^k\bar{\Psi}(\tilde{n})\,\mathrm{d}\tilde{n},$$

$$\bar{\Psi}(\tilde{n}) = \int_0^{\tilde{n}} \frac{k+1}{\tilde{r}^k a_2(\tilde{n})}\int_0^{\bar{n}} \tilde{u}\tilde{r}^k\,\mathrm{d}s\,\mathrm{d}\bar{n}. \tag{A.10}$$

From this, one finally derives for Eq. (A.5)

$$\sum_{i=1}^{\infty}\frac{\Phi_{i1}(1)\Phi_{i1}(\tilde{n})}{\lambda_i^2\left\|\vec{\Phi}_i\right\|^2} = \Psi(\tilde{n}) = \bar{\Psi}(\tilde{n}) + C_2. \tag{A.11}$$

It should be noted here, that the found analytical expressions for the two sums, according to the Eqs. (A.1) and (A.5), will transform into the expressions developed by Papoutsakis et al. [5] if we consider the simplified case of laminar pipe flow ($k=1$, $a_1 = a_2 = 1$, $\tilde{u} = 2(1-\tilde{n}^2)$). For this case, one obtains

$$\begin{aligned}\sum_{i=1}^{\infty}\frac{\Phi_{i1}(\tilde{n})\Phi_{i1}(1)}{\lambda_i\left\|\vec{\Phi}_i\right\|^2} &= 2,\\ \sum_{i=1}^{\infty}\frac{\Phi_{i1}(1)\Phi_{i1}(\tilde{n})}{\lambda_i^2\left\|\vec{\Phi}_i\right\|^2} &= \tilde{n}^2 - \frac{\tilde{n}^4}{4} + \frac{8}{Pe_D^2} - \frac{7}{24}.\end{aligned} \tag{A.12}$$

References

[1] R.K. Shah, A.L. London, Laminar Flow Forced Convection in Ducts, Academic Press, New York, 1978 (Chapters V and VI).

[2] M.S. Bhatti, R.K. Shah, in: S. Kakac, R.K. Shah, W. Aung (Eds.), Turbulent and Transition Flow Convective Heat Transfer in Ducts, Wiley, New York, 1987 (Chapter 4).

[3] D.K. Hennecke, Heat transfer by Hagen–Poiseuille flow in the thermal development region with axial conduction, Wärme- und Stoffübertragung 1 (1968) 177–184.

[4] C.J. Hsu, An exact analysis of low Peclet number thermal entry region heat transfer in transversally nonuniform velocity fields, AIChE J. 17 (1971) 732–740.

[5] E. Papoutsakis, D. Ramkrishna, H.C. Lim, The extended Graetz problem with prescribed wall flux, AIChE J. 26 (1980) 779–787.

[6] E. Papoutsakis, D. Ramkrishna, H.C. Lim, The extended Graetz problem with Dirichlet wall boundary conditions, Appl. Sci. Res. 36 (1980) 13–34.

[7] T.V. Nguyen, Laminar heat transfer for thermally developing flow in ducts, Int. J. Heat Mass Transfer 35 (1992) 1733–1741.

[8] S. Bilir, Numerical solution of Graetz problem with axial conduction, Numer. Heat Transfer, Part A 21 (1992) 493–500.

[9] C.B. Reed, Convective heat transfer in liquid metals, in: S. Kakac, R.K. Shah, W. Aung (Eds.), Handbook of Single-Phase Convective Heat Transfer, Wiley, New York, 1987 (Chapter 8).

[10] S.L. Lee, Liquid metal heat transfer in turbulent flow with uniform wall flux, Int. J. Heat Mass Transfer 26 (1983) 349–356.

[11] N.Z. Azer, B.T. Chao, A mechanism of turbulent heat transfer in liquid metals, Int. J. Heat Mass Transfer 1 (1960) 121–138.

[12] B. Weigand, An exact analytical solution for the extended turbulent Graetz problem with Dirichlet wall boundary conditions for pipe and channel flows, Int. J. Heat Mass Transfer 39 (1996) 1625–1637.

[13] S. Faggiani, F. Gori, Influence of streamwise molecular heat conduction on the heat transfer for liquid metals in turbulent flow between parallel plates, J. Heat Transfer 102 (1980) 292–296.

[14] C.C. Chieng, B.E. Launder, On the calculation of turbulent heat transfer downstream from an abrupt pipe expansion, Numer. Heat Transfer 3 (1980) 189–207.

[15] A.J. Reynolds, The prediction of turbulent Prandtl and Schmidt numbers, Int. J. Heat Mass Transfer 18 (1975) 1055–1069.

[16] B. Weigand, J.R. Ferguson, M.E. Crawford, An extended Kays and Crawford turbulent Prandtl number model, Int. J. Heat Mass Transfer 40 (1997) 4191–4196.

[17] H. Fuchs, Wärmeübergang an strömendes Natrium, PhD Thesis, Eidg. Institut für Reaktorforschung, Würenlingen, Switzerland, EIR-Bericht, no. 241, 1973.